water

MDPI

Article

An Effective Standalone Solar Air Gap Membrane Distillation Plant for Saline Water Desalination: Mathematical Model, Optimization

Nawel Mibarki [1], Zakaria Triki [1], Abd-Elmouneïm Belhadj [1], Hichem Tahraoui [1,2], Meriem Zamouche [3], Mohammed Kebir [4], Abdeltif Amrane [5,*], Jie Zhang [6] and Lotfi Mouni [7,*]

1 Laboratory of Biomaterials and Transport Phenomena, University of Medea, Medea 26000, Algeria
2 Laboratoire de Génie des Procédés Chimiques, Department of Process Engineering, University of Ferhat Abbas, Setif 19000, Algeria
3 Laboratoire de l'Ingénierie des Procédés de l'Environnement (LIPE), Faculté de Génie des Procédés, Département de Génie de l'Environnement, Université de Constantine 3, Constantine 25000, Algeria
4 Research Unit on Analysis and Technological Development in Environment (URADTE-CRAPC), Tipaza 42000, Algeria
5 Ecole Nationale Supérieure de Chimie de Rennes, Université de Rennes, CNRS, F-35000 Rennes, France
6 School of Engineering, Merz Court, Newcastle University, Newcastle upon Tyne NE1 7RU, UK
7 Laboratory of Management and Valorization of Natural Resources and Quality Assurance, SNVST Faculty, Université de Bouira, Bouira 10000, Algeria
* Correspondence: abdeltif.amrane@univ-rennes1.fr (A.A.); l.mouni@univ-bouira.dz (L.M.)

Abstract: Several drinking water production techniques are being established to respond immediately to the growing needs of the population. The system of air gap membrane distillation (AGMD) is the best attractive option for the process of water desalination. This thermal process is characterized by its potential to provide drinking water at low energy costs when combined with solar energy. In this paper, the AGMD brackish water desalination unit potentialities coupled with solar energy were investigated. Ghardaïa of the south region has been considered as the field of our study. Mathematical modeling is investigated by employing MATLAB software to develop the prediction of the permeate flux related to the phenomena of heat and mass transfer. Herein, flat plate solar collectors (SFPC) were exploited as a source for heating saline water through free solar energy conversion. The further model validation of a flat solar collector made it possible for following the instantaneous evolution of the collector outlet temperature depending on the feed water temperature and the flow rate. Furthermore, it is interesting to note that the results prove the possibility to produce water by the solar AGMD process with a maximum permeate flux of 8 $kg \cdot m^{-2} \cdot h^{-1}$ achieved at 68 °C, a feed temperature. Moreover, gained output ratio (GOR) of the unit of thermal solar desalination was estimated to be about 4.6, which decreases with increasing hot water flow and temperature.

Keywords: brackish water desalination; flat plate collector; membrane distillation; modeling; performance; solar energy

check for updates

Citation: Mibarki, N.; Triki, Z.; Belhadj, A.-E.; Tahraoui, H.; Zamouche, M.; Kebir, M.; Amrane, A.; Zhang, J.; Mouni, L. An Effective Standalone Solar Air Gap Membrane Distillation Plant for Saline Water Desalination: Mathematical Model, Optimization. *Water* **2023**, *15*, 1141. https://doi.org/10.3390/w15061141

Academic Editor: Carmen Teodosiu

Received: 22 January 2023
Revised: 12 March 2023
Accepted: 13 March 2023
Published: 15 March 2023

1. Introduction

Recently, solar energy is a green alternative source that can help to avoid the need for global power for current and future consumption. Moreover, it provides multiple applications, including the food industry, space heating, and water heaters. Solar collectors operate as heat exchangers that transmit heat from the sun's radiant energy to the medium of fluid (air or water). They can be considered an important component of dynamic solar-heating systems, such as solar pool heating systems, space heating systems, and systems for heating water and spaces [1,2].

Because of its potential and performance, the solar flat plate solar collector (SFPC) is currently one of the most popular devices used for converting solar energy into thermal energy, which can be used in multiple cases, for example, hot and cold water production and air conditioning. Meanwhile, solar distillation received great attention due to its advantages of a straightforward structure, a high-pressure bearing, durability, ease of maintenance, excellent heat efficiency, and low energy costs. From a renewed interest, it will become more suitable for sustainable water production, and the principal tendency going forward is to overcome the growing need for solar energy process integration in buildings [3,4].

The Algerian Sahara, which extends from the Saharan Atlas mountains, has a surface area of more than two million square kilometers and borders Mali, Niger, and Libya, and is considered to be the largest and driest place on earth. With an estimated population of three and a half million people, most of whom are centered in the Wilaya major localities, it covers a distance over two 2000 km (north–south), some of which reach 150,000 ca. erg. Regs and saline lakes, which are enormous bodies of water unfit for agriculture, make up the majority of this vast land [5].

Ghardaia is located in the Algerian north desert, and it belongs to an arid area, which records daily global solar radiation (GSR) changes from 607 to 7574 $Wh{\cdot}m^{-2}/day$ when the annual-mean-daily GSR reached 5656 $Wh{\cdot}m^{-2}/day$. This region has its place in the great solar deposit characterized by tremendous advances in a vast array of alternative renewable energy options, including solar power, which is a very important means for developing desalination technologies, such as membrane distillation (MD). Recently, the latter has encountered a specific interest in its applications in the water desalination field, particularly when paired with solar power [6].

In the literature, four main types of MD configurations, which differs in the permeate treatment nature: Direct contact membrane distillation (DCMD), vacuum membrane distillation (VMD), air gap membrane distillation (AGMD), and sweeping gas membrane distillation (SGMD). AGMD is the most adaptable of all membrane distillation setups because of its gas gap. This configuration is distinguished from the others set up by low thermal losses and a low-risk possibility of wetting and clogging of the membrane. Additionally, when comparing the benefits and drawbacks of various DM configurations, the AGMD appears to be the ideal option for coupling with a solar FPC since its uses are reducing energy consumption and thereby increasing the faster permeate recovery [7,8].

Solar energy devices were used in the design and testing of the MD units, such as SFPC [9,10], vacuum tube collector [11,12], compound parabolic collector (CPC) [13], solar ponds [14,15], and solar still [16,17]. Banat's team has worked extensively on solar-powered membrane distillation (SPMD) [9,10,16,18,19] and set up compact SPMD units in arid and semi-arid regions far away from Jordan. The spiral-wound AGMD module with an internal heat recovery mechanism was made up of the desalination system. The energy is supplied by the SFPC, while a PV panel provided the auxiliary electricity.

Elena Guillén-Burrieza et al. [20] carried out an experimental evaluation of a pilot solar desalination system based on AGMD configuration with a total membrane surface area per module of 2.8 m^2. A feeding solution of NaCl with 1 and 35 $g{\cdot}L^{-1}$ concentrations was used. Specific distillate flux was displayed by modules of AGMD with values up to a maximum of 6.5 $L{\cdot}m^{-2}{\cdot}h^{-1}$ at 65 °C feedwater temperature and for 1 $g{\cdot}L^{-1}$ of NaCl feed solution. Kubota et al. [21], in their study, reported distillate fluxes of about 4.7 $L{\cdot}h^{-1}{\cdot}m^{-2}$ for a system made up of an AGMD module of 1.92 m^2 of membrane, a feed flow rate of 20 $L{\cdot}min^{-1}$, and 40 °C feed water temperature, while Banat et al. [10] reported that a distillate fluxes up to 2.5 $L{\cdot}m^{-2}{\cdot}h^{-1}$ for a larger system composed of 4 MD modules of 10 m^2 of each membrane, a feed flow rate up to 21.2 $L{\cdot}min^{-1}$, and 74 °C feed temperature; in both investigations, they used real seawater.

Edward K. Summers et al. [22] presented a novel AGMD design that employs a direct solar energy source heating of the MD membrane. This configuration provides a more homogenous temperature profile over the membrane in the flow direction, thereby improving the production of vapor. The acquired results showed that it is capable of achieving thermal efficiencies that are almost twice as high as those of current MD systems that are powered by solar energy.

In another research, D. Moudjeber et al. [23] conducted a study in which a commercial membrane distillation module was used. This later has an AGMD and spiral-wound configuration. Experiments have been carried out concerning the simulation of the salinity and temperature of the water. For this purpose, the Albian aquifer of Algeria is taken as a case study. The maximum value of distillate production was 5 $L \cdot h^{-1}$ m^{-2} for 34.5 °C of the temperature of the feed water with a salinity of 4 $g \cdot L^{-1}$.

Additionally, N.T. Uday Kumara et al. [24] characterized experimentally a semi-commercial AGMD module under different operating parameters. Furthermore, a numerical optimization was also performed by the authors in order to gain insight into the set of optimizing conditions that would further be useful for achieving the desired operation. It was found that for the required distillate flux of 15 $L \cdot m^{-2} \cdot h^{-1}$, MD hot and cold temperature difference must be kept between 40 °C and 45 °C, while it is necessary to adjust the flow rate from 6 to 7 $L \cdot min^{-1}$ depending upon the operating season.

Similarly, Ganesh B. Shirsath et al. [25] realized a single stage and four stages of AGMD coupled by means of a horizontal solar device. The obtained results from mathematical modeling indicated that the multistage AGMD system could deliver nearly four times as much water as the single-stage system. In addition, the outcomes of using a hydrophobic membrane to improve the water productivity from solar still were further confirmed by experimental study results.

Recently, Abdelfatah Marni Sandid et al. [26–28] conducted several investigations on solar desalination via AGMD using the TRNSYS tool. First, they simulated a single cassette AGMD module by integrating the solar thermal unit. According to the obtained data, when the inlet AGMD temperature reaches 85 °C, the distilled water flow from the distillation membrane achieves 5.5 $kg \cdot h^{-1}$ and remains nearly constant on various days during the year by utilizing solar energy alone. Afterward, a pilot-scale experiment study was carried out to determine the performance of a 14.4 m^2 multichannel spiral-wound AGMD module, which can be used for water desalination with capacities up to 18 $kg \cdot h^{-1}$ from the flow rate of distillate water. The AGMD system's specific thermal energy consumption ranged from 158.83 to 346.55 $kWh \cdot m^{-3}$, and the maximum gain output ratio (GOR) achieves 4.4 at 52 °C, based on the inlet temperature of feed.

In recent years, optimization algorithms have become an essential tool for a large variety of applications in many fields, including machine learning, engineering, finance, and scientific research. These algorithms help to find the best possible solution or set of solutions for a given problem, which can lead to improved efficiency, accuracy, and effectiveness in a wide range of applications. Description of design and optimization algorithms could be found in the following papers: [29–31]. Numerous investigations have explored how to optimize AGMD by identifying the most effective variable values, resulting in improved outcomes [32–34]. The studies have consistently found that air gap thickness is a crucial element in the desalination process, and better results are obtained when the air gap is thinner, especially with regard to flow permeation [35–37].

This study's goal is to simulate and enhance the solar AGMD desalination system achievements applied to the desalination of saltwater using meteorological data of the Ghardaïa region (South of Algeria). Furthermore, the effects of instantaneous temperature change at the collector output on permeate flow rate, solar radiation, and feed water temperature were investigated. Finally, based on the heat and mass transfer energy balance, equations for each part of the solar desalination system, specifically the AGMD module, the solar collector, the heat exchanger and the tank, the temperature change, and the amount of distillate produced at the outlet of the module were determined.

2. System Description

The schematic diagram in Figure 1 represents the process of attempting the production of high-quality distilled water with minimal consumption of energy. A SFPC is coupled to an AGMD unit by a plate heat exchanger. Preheating the feed solution is necessary to recover the amount of heat that is present in the brine. Therefore, to limit the evolution of the feed temperature in the tank, a plate heat exchanger is inserted between the AGDM unit and SFPC. Additionally, a pump was successively processed to drive the feed solution in the cold channel of the desalination unit, and then in the hot channel of the AGMD unit wherever the flow is divided into permeate flow and brine flow, which is a slightly more concentrated salt, the brine finally flows to the supply tank. The combination of the SFPC will give this system operational autonomy.

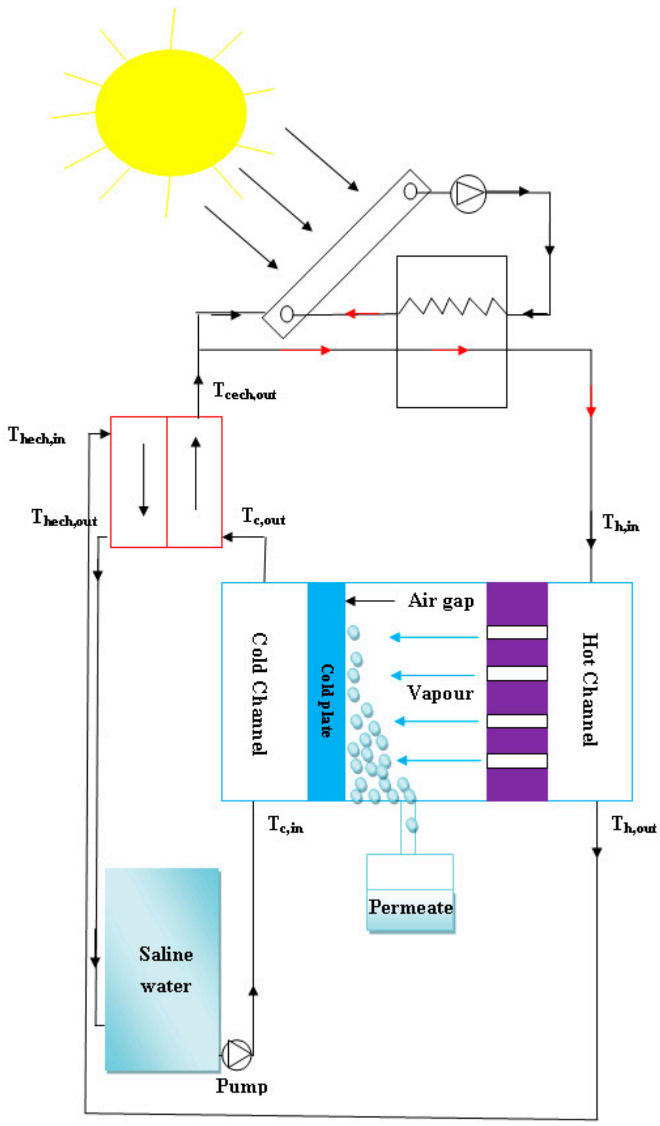

Figure 1. Schematic diagram of the AGMD process.

In order to extract the heat from sunlight, a solar collector is employed. Additionally, at the heart of a solar collector is a menu of a solar absorber. The latter absorbs the sun's radiation and converts it into heat. Such installations combining these innovative technologies can find applications in the navy, emergency medical aid, or improving the living conditions of populations in isolated sites. The aim is the extraction of heat from a heat exchanger submerged in a storage tank connected with a flat solar collector in closedcycle continuous flow heating modes and therefore using this energy for the desalination of saline water.

3. Numerical Modeling and Proposed Method

MATLAB software was used for modeling the solar AGMD system. Accordingly, a series of mathematical calculations were performed based on the design parameters described later in order to analyze the performance of the solar AGMD system under different operating conditions.

3.1. AGMD Unit

The principle of AGMD is to separate a feed compartment from a permeate compartment using a microporous and hydrophobic membrane. Two transfer phenomena occur simultaneously inside the AGMD configuration module: heat and mass. The equations of heat and mass transfer, as well as the literature correlations, were used to create the 1D model [8].

3.1.1. Heat Transfer

Within an AGMD module, heat transmission by convection and conduction are the two most common forms of heat transfer. Irradiative heat transmission is frequently overlooked. Heat is transmitted into the hot channel, inside the membrane's pores, in the air gap, on the cold plate's surface, in the cold channel, and between the cold liquid and the cold plate's surface. In the unit Equation (1), energy conservation is used. However, the quantity of energy lost in the permeate flow as well as heat losses over the plastic of the AGMD unit's exterior walls to the environment are not taken into account [8].

$$\varphi_h = \varphi_m = \varphi_{ag} = \varphi_p = \varphi_c \tag{1}$$

where h_{ch} is the coefficient of convective exchange and T_h is the differential temperature between the hot solution temperature, and T_{hm} is the temperature of the hot solution at the interface of the membrane. Equation (2) is used to determine the heat flow in the hot channel, where R_{mT} is the membrane's thermal resistance, T_{mg} is the temperature at the membrane-air gap interface, J_v is the vapor flux traveling through the membrane, and h_v is the evaporation enthalpy [38].

$$\varphi_h = h_{ch}(T_h - T_{hm}) \tag{2}$$

A convective term plus a diffusive term make up the heat flux from the membrane surface to the condensate. The following equation, Equation (3), governs the situation [39]:

$$\varphi_m = \frac{1}{R_{mT}}(T_{hm} - T_{mg}) + J_v \Delta h_v \tag{3}$$

Heat flow across an air gap is calculated using Equation (4), where R_{ag} and T_p are the air gap thermal resistance and the permeate temperature, respectively [8].

$$\varphi_{ag} = \frac{1}{R_{ag}}(T_{mg} - T_p) \tag{4}$$

The following equation can be used to calculate the heat flux in the cold channel's boundary layer, where h_{cc} and T_c are the coefficient of heat transfer and the cold solution temperature in the cold channel, respectively. The heat flux in the cold channel's boundary layer, as shown in Equation (5) [38]:

$$\varphi_c = h_{cc}(T_p - T_c) \tag{5}$$

3.1.2. Mass Transfer

The mass transfer through the membrane is determined by the difference in vapor pressure between the two sides of the membrane. In the AGMD process, the permeate flux (J_w) is proportional to the vapor pressure difference throughout the membrane matrix, and it can be calculated using Equation (6) [8,40], where P_{hm} and P_p are the vapor pressures at the membrane's surface in the hot channel's boundary layer and the air gap at the cooling plate's surface, respectively. α is the activity coefficient and is the solution's water fraction.

$$J_w = B_w \left(\alpha \beta P_{hm} - P_p \right) \tag{6}$$

To explain and calculate the pressures P_{hm} and P_p, the Antoine equation can be used and is given by Equation (7) [8]:

$$P = \exp\left(23.1964 - \frac{3816.44}{T - 46.13} \right) \tag{7}$$

In Equation (6), the membrane permeability or the mass transfer coefficient B_w is given in Equation (8). Water molecular weight, gas constant, absolute membrane temperature, and total pressure inside the pores are all represented by M_w, R, T_m, and P, respectively. D_{va} is the water vapor's thermal diffusivity in the air gap, and τ is the membrane's tortuosity [8].

$$B_w = \frac{\varepsilon M_w P D_{va}}{R T_m \left(\delta_m \tau + \delta_{ag} \right) |P_a|_{ln,a}} \tag{8}$$

The mass flow rate of the AGMD module is given by Equation (9), where J_w and S_m are the permeate flux and membrane surface, respectively, as shown in Equation (10) [38].

$$\dot{m}_p = J_w . S_m \tag{9}$$

The value of the vapor flux is determined by combining the transfer and mass equations developed previously. The MATLAB program was used to calculate the heat transfer and, hence, the permeate flux. Figure 2 shows the flowchart for calculating the permeate mass flow.

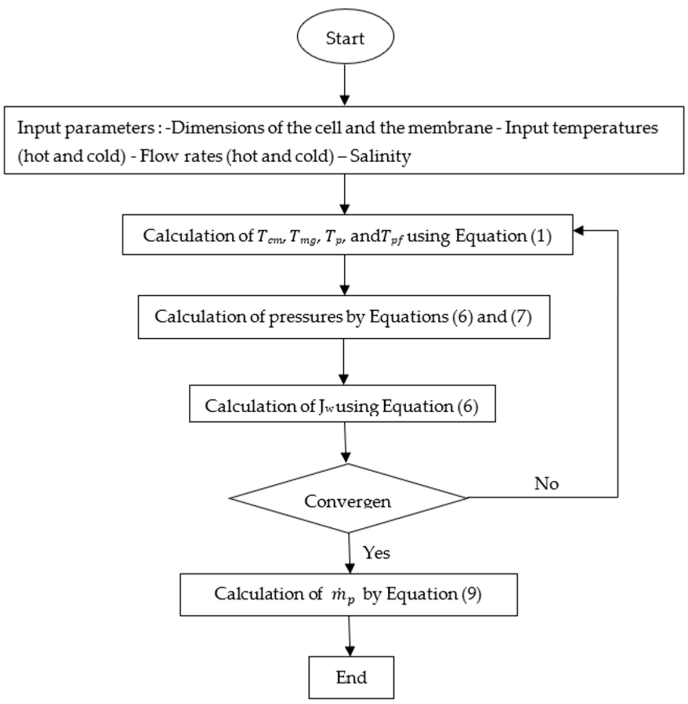

Figure 2. Flowchart of mass flow calculation.

Figure 3 presents the strategy for simulating a flat plate collector coupled to an AGMD unit. Initial water conditions must be given for heat transfer calculations. Thus, the inlet temperature of the sea water to the solar collector corresponds to the outlet temperature of the cold channel of the MD cell and the outlet temperature of the water in the solar collector to that of the inlet temperature of the hot channel.

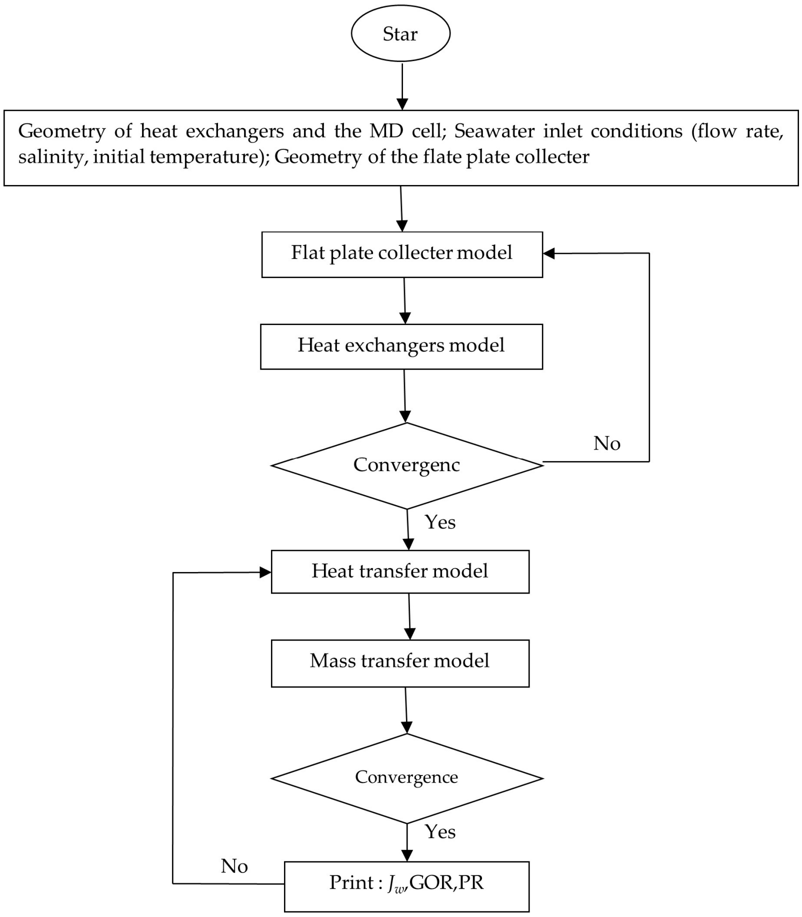

Figure 3. Flowchart of the optimal design.

3.2. Heat Exchangers Model

In heat exchanger models, the logarithmic average of temperature differences is used (LMDT). Equations (10)–(12) can be applied to compute the heat exchanged [8].

$$\Phi = F.U.A.\text{LMDT} \tag{10}$$

$$\Phi = \dot{m}_{so}.C_{p,so}.A.\Delta T_{so} \tag{11}$$

$$\Phi = \dot{m}_r.\Delta h_r \tag{12}$$

3.3. Solar Flat Plate Collector

When solar radiation passes through the blanket, it gains energy for the collector. The energy gained by the absorber may be calculated by Equation (13) [41]:

$$Q_r = (\alpha\tau)_{eff}.I_T \tag{13}$$

with $(\alpha\tau)_{eff}$ denoting the effective optical fraction of the absorbed energy, I_T is the total amount of solar radiation incident on the collector surface in W/m^2, and A_c is the collector surface in m^2.

The obtained energy by the collector can be expressed by Equation (14) [41]:

$$Q_i = I_T \times A_c \tag{14}$$

The heat loss rate Q_0 is determined by the collector's total heat transfer coefficient U_L and its temperature. It can be expressed by Equation (15) [42]:

$$Q_0 = U_L \times A_c(T_c - T_a) \tag{15}$$

where Q_0 represents the heat loss in W, U_L represents the heat loss coefficient W/K·m^2, T_c represents the collector's average temperature in °C, and Ta represents the ambient temperature in °C. As a result, the rate at which the collector extracts useful energy, denoted as the extraction rate under stable state conditions, is proportional to the amount of useful energy absorbed by the collector minus the quantity lost by the collection. It is written as shown in Equation (16) [41]:

$$Q_u = Q_r - Q_0 = (\alpha\tau)_{eff}.I_T.A_c - U_L.A_c(T_c - T_a) \tag{16}$$

The term for the increase in actual usable energy of a collector surface at the fluid's inlet temperature is straightforwardly defined. The collector heat removal factor (FR) is reported by Equation (17) [43]:

$$FR = \frac{\dot{m}C_p(T_0 - T_i)}{(\alpha\tau)_{eff}.I_T.A_c - U_L.A_c(T_c - T_a)} \tag{17}$$

When the assembly sensor is at the temperature of the inlet fluid, the solar collector produces the most beneficial energy gain. By multiplying the collector's heat removal factor (FR) with the greatest useful energy gain feasible, the real useful energy gain Q_u is derived as shown in Equation (18) [41,44]:

$$Q_u = FR.A_c\left[(\alpha\tau)_{eff}.I_T. - U_L(T_i - T_a)\right] \tag{18}$$

The ratio of usable energy gain Q_u on incident solar energy corresponds to the collector's efficiency, as shown in Equation (19) [43].

$$Q_u = FR.(\alpha\tau)_{eff} - \left[\frac{FR \times U_L(T_i - T_a)}{I_T}\right] \tag{19}$$

3.4. System Performance Assessment

For desalination units, their performance is evaluated according to the amount of energy consumed relative to the generated amount of freshwater. The GOR (gained output ratio) corresponds to the ratio of the required energy amount to evaporate the permeate flux divided by the heat consumption; it is used to measure the energy consumption of the process, and it can be described by Equation (20).

The GOR is a dimensionless ratio that can be stated as an energy or a mass ratio, and it is used in processes for thermal desalination. It is frequently defined as the energy ratio of the total latent heat produced by the water to the thermal energy input [45,46].

$$\text{GOR} = \frac{\dot{m}_p.\Delta h_v}{\dot{m}_{sw}.C_{p,sw}.(T_{h,in} - T_{h,out})} \tag{20}$$

where $\dot{m}_p$ is the mass of the produced permeate, Δh_v is the latent heat of vaporization, $\dot{m}_{sw}$ is mass flow rate of seawater, $C_{p,sw}$ is the specific heat of feed, and $T_{h,in}$ and $T_{h,out}$ are temperature inlet and outlet of the hot side of the module, respectively.

A desalination system's performance ratio (PR) is defined as the mass of distillate to the energy input, and it is calculated by Equation (21) [39]:

$$\mathrm{PR} = \frac{\dot{m}_p}{Q_u} \tag{21}$$

where $\dot{m}_p$ is the mass of the produced permeate, and Q_u is the consumption of thermal or electrical energy.

4. Results and Discussion

4.1. Validation of the AGMD Model

In this study, the validation of the prediction model was performed based to the experimental results obtained by Diaby et al. [38]. The evolution of the predicted and measured water vapor flow was compared at different feed water temperatures. Figure 4 demonstrates that the evolution of the permeate flow is affected by the temperature of the feed water. Furthermore, it was noticed that increasing the feed temperature of the permeate flow grows exponentially. At these temperatures, the permeate flow goes from 0.625 to 7.03 kg·m^{-2}·h^{-1} at a cooling temperature set at 15 °C and a cooling flow rate set at 5 L·min^{-1}. This change in permeate flow may be the result of the water vapor's increased transmembrane force. The outcomes are consistent with those that have been reported by many authors in the literature [47,48].

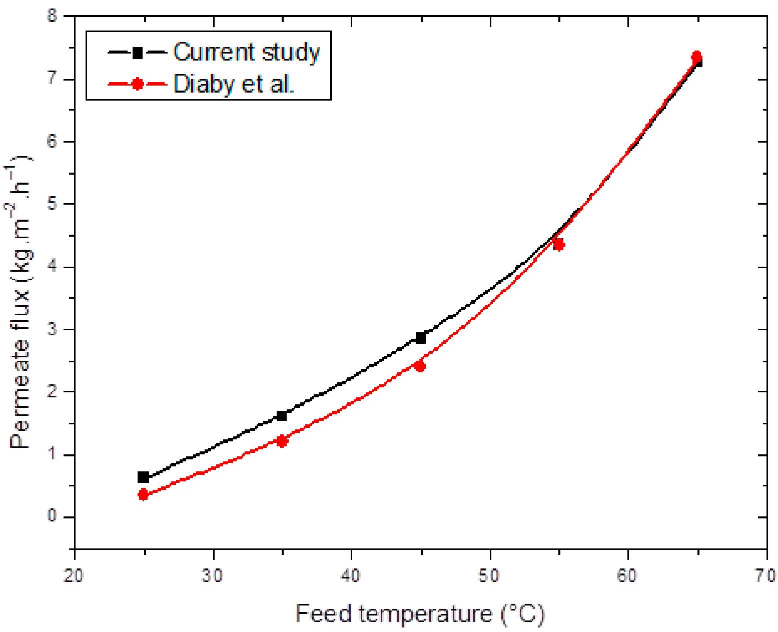

Figure 4. Evolution of permeate flux as a function of feed temperature [38].

A literature search of the AGMD system revealed wide discrepancies in the values. Table 1 summarizes permeate flux for some MD configurations.

Table 1. Summary of permeate flux for different MD configurations from the literature.

MD Type	Membrane Type	Pore Size	Solution	Feed Teperature (°C)	J_w (kg·m^{-2}·h^{-1})	Reference
AGMD	PVDF	0.22	Methanol/water	50	≈3.9–4.6	[49]
AGMD	PTFE	0.2	NaCl	65	≈7	[8]
AGMD	PTFE	0.2	NaCl	80	≈6.5	[47]

Table 1. *Cont.*

MD Type	Membrane Type	Pore Size	Solution	Feed Teperature (°C)	J_w (kg·m^{-2}·h^{-1})	Reference
VMD	PP	0.2	NaCl	55	≈10.7–7.0	[50]
DCMD	PTFE	0.2	NaCl	31	≈32.4–25.2	[51]
DCMD	PVDF	0.4	NaCl	81	≈44–63	[52]
DCMD	PVDF	0.22	NaCl	68	≈36–28.8	[53]
AGMD	PTFE	0.2	NaCl	65	7.03	Current study

4.2. Evaluation of Solar Potential

To assess the region's solar potential for the current study, a radiometric station using high precision to measure the data for solar radiation has been installed on the roof of the solar radiation laboratory of the applied research unit for renewable energies (URAER) building in the region of Ghardaia [54]. A set of 335 days during the year (9 February–31 December) has been used to record the solar radiation and temperature as depicted in Figure 5. It can be noticed that the highest temperature of 38 °C was recorded in July, and the lowest one of 11 °C was recorded in January. Therefore, the month of July is considered the most suitable period for this study.

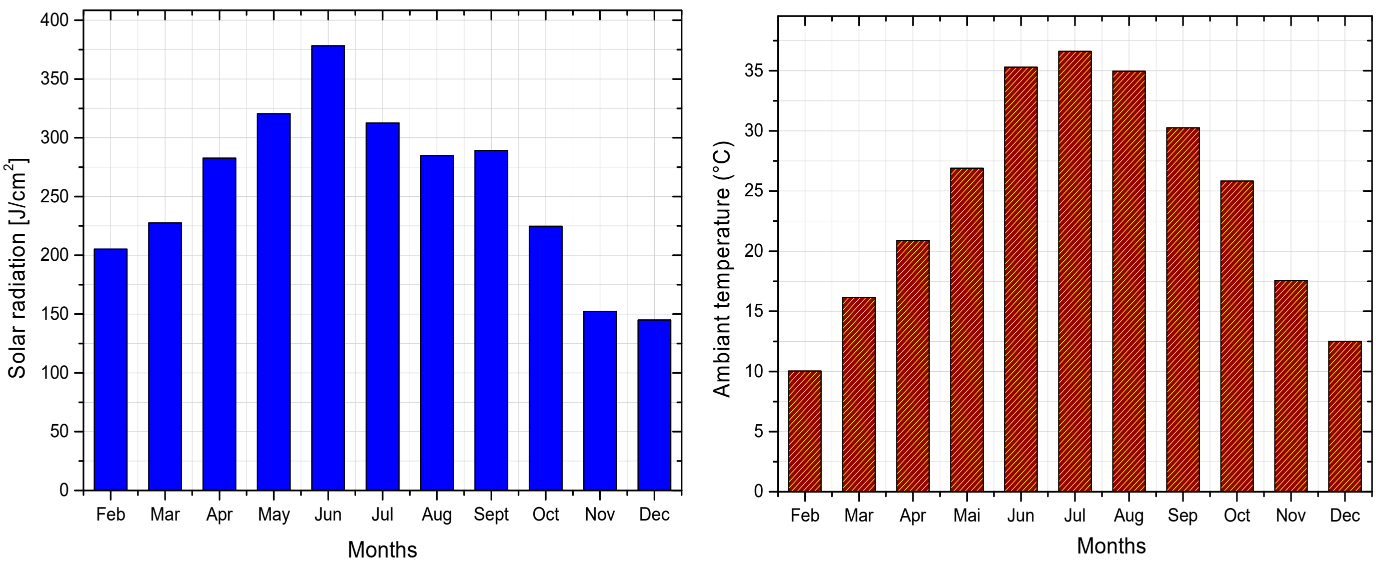

(**a**) Solar radiation (**b**) Temperature

Figure 5. Annual solar radiation and ambient temperature evolution (Ghardaïa site).

Figure 6 shows the global solar daytime irradiation evolution for the months June, July, and August. The irradiation distribution has a bell-shaped profile that is consistent with the prediction of well-known semi-empirical models from the literature. It is also noticed that the highest temperature and solar radiation values are recorded on 21 July , which is the most appropriate day to be considered in the present work.

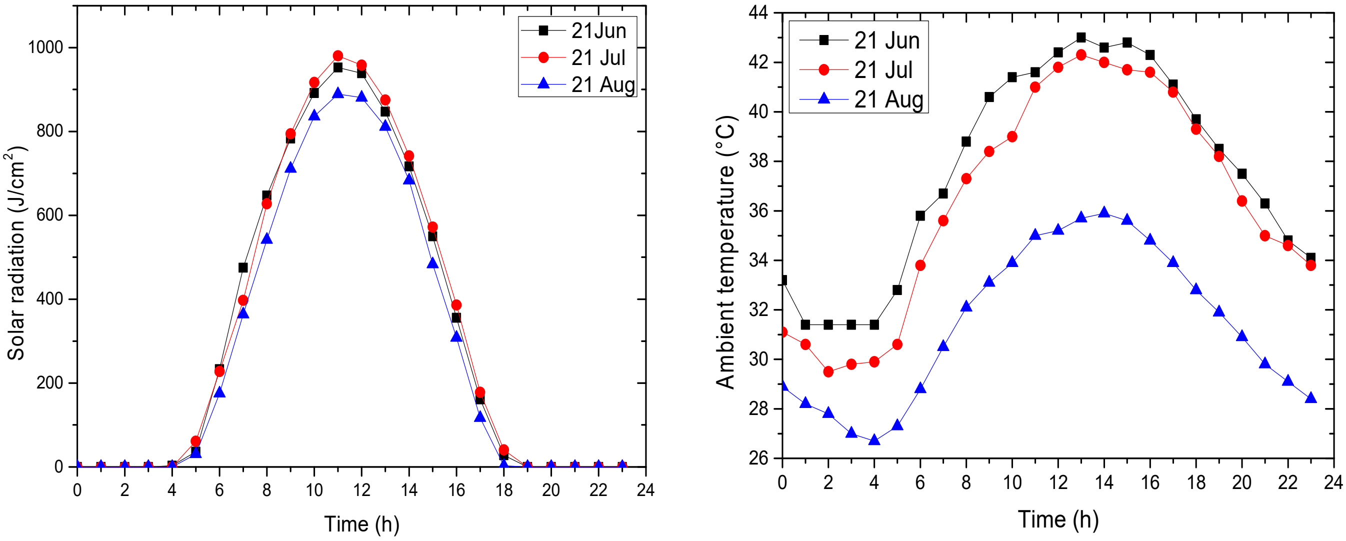

(**a**) Solar radiation (**b**) Temperature

Figure 6. Instantaneous variation of solar radiation and ambient temperature (Ghardaïa site).

4.3. Variation of the Temperature in AGMD Unit

Generally, the heat transfer is involved by two dominant modes inside the AGMD module, convection and conduction, while heat transfer by radiation is the most often overlooked. The equation of energy conservation was used to calculate the temperature at the interface of the hot feed solution and membrane surface (T_{hm}), the temperature at the interface between the membrane and the air gap (T_{mg}), the temperature of permeate (T_p), and the temperature at the interface between the cooling solution and the cold plate's surface (T_{pc}). The obtained results are given in Figure 7.

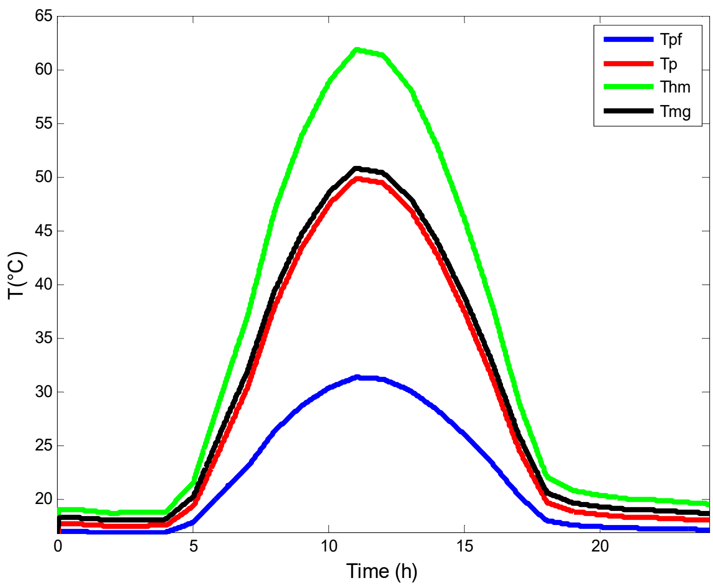

Figure 7. Variation of AGMD operating temperatures with time.

The graph below shows the time-dependent variation in saline temperature at the counter-current plate heat exchanger's input and outflow (Figures 8 and 9) As can be seen, when the solar flux increases, the temperature of the saline water at the exit of the heat exchanger increases. Additionally, the feed fluid temperature that increase in the morning reach a maximum peak of 58 °C between 12 and 14 h and then drops in the afternoon.

This value is considered as a typical feed temperature range for the AGMD process, which varies between 40 °C and 80 °C [55].

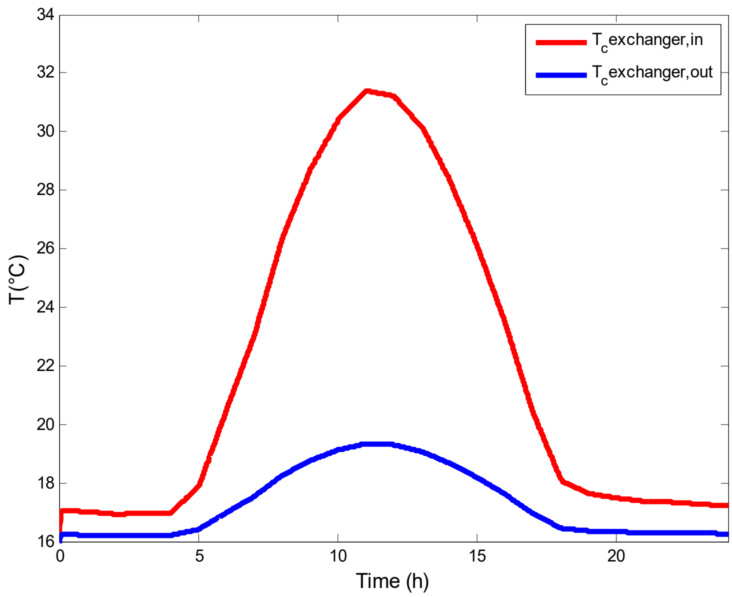

Figure 8. Saline water temperatures variation at the level of a plate heat exchanger with time.

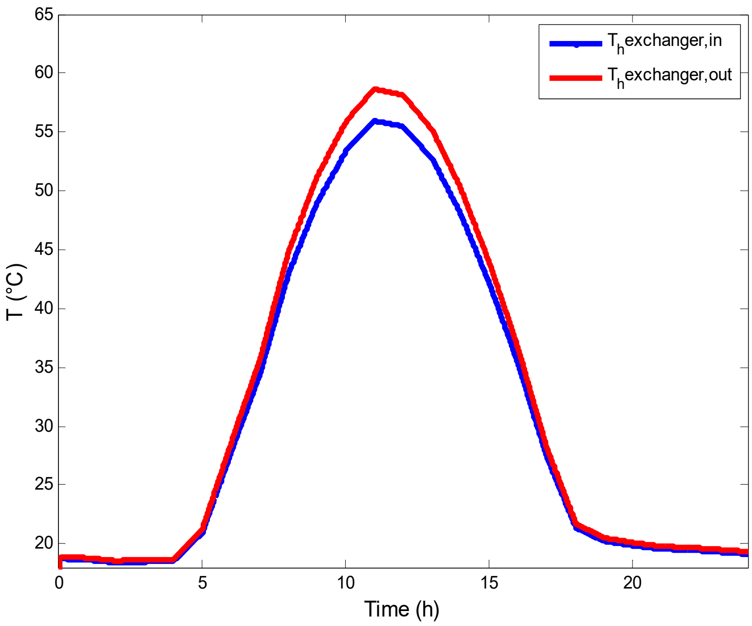

Figure 9. Variation of saline water temperatures at the level of a plate heat exchanger with time.

4.4. Variation of the Saline Water Temperature in Flat Plate Collector

Flat plate collectors' outgoing heat-transfer fluid temperature varies depending on the local time, as seen in Figure 10. As anticipated, the heat-transfer fluid temperature leaving the flat plate collectors rises to a maximum of roughly 50 °C in accordance with the solar flux rate; this value is the most suitable temperature for the AGMD process and the collector's safety.

The obtained result shown in Figure 11 indicate that the saline water temperature increases with time when the saline water is heated inside the tank to reach a maximum value around of 60 °C for a 0.01 kg·s^{-1} mass flow rate.

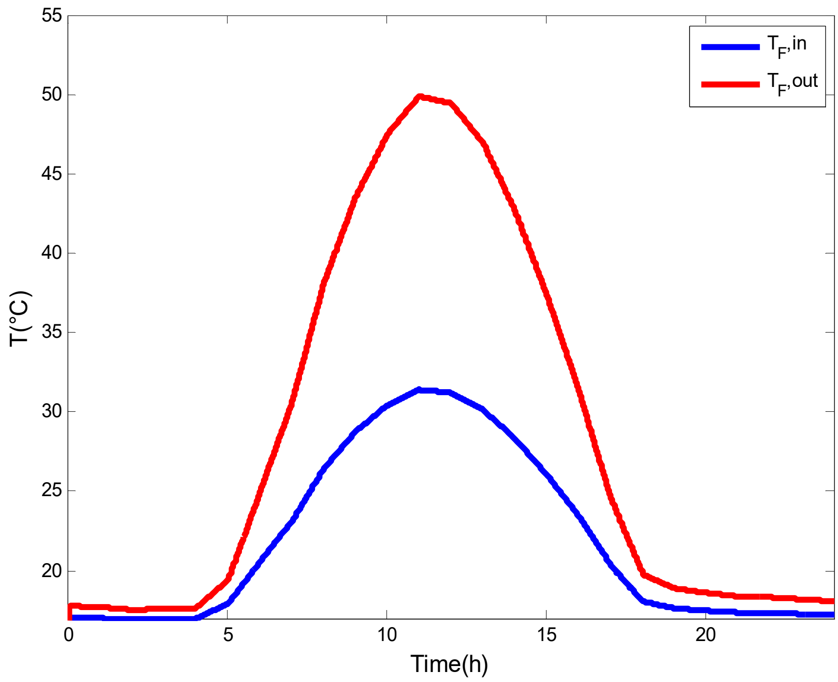

Figure 10. Variation of the inlet and outlet of the heat transfer fluid temperatures from the flat plate collector with time.

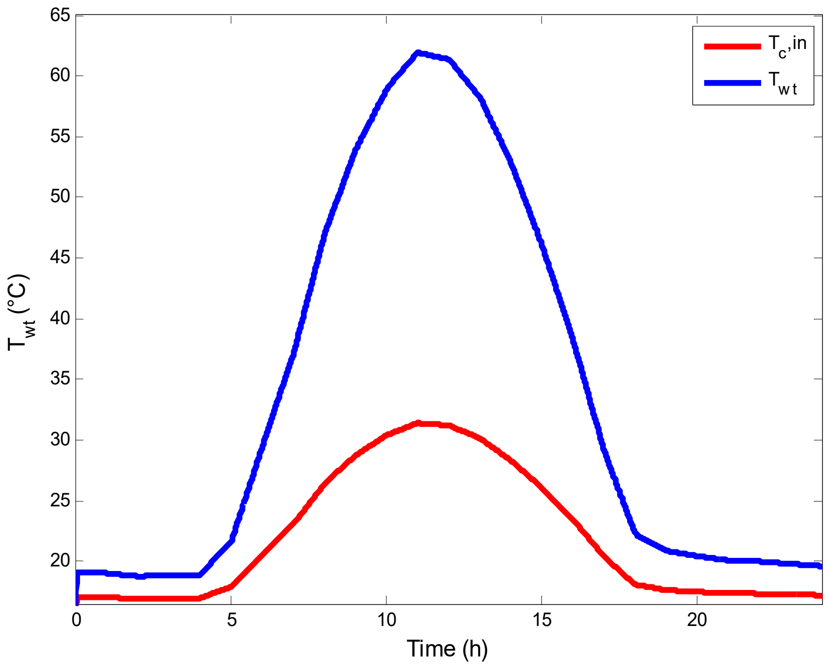

Figure 11. Variation of the inlet and outlet of saline water temperatures in the tank with time.

4.5. Variation of the Permeate Flux

Figure 12 shows the permeate flux evolution with the local time. As can be seen, the permeate flux growths at the beginning of the day reach about 8 kg·m^{-2}·h^{-1} for a flow rate of 0.01 kg·s^{-1} and is considered as the maximum value goshawk 12:00 h. These obtained results show the best matching with the other results cited in the literature. As can be observed from Figure 13, the permeate flux is very sensitive to the variation of the flow rate of seawater. It was marked that the permeate flux increases as the flow rate of seawater decreases. Permeate flux passes from 8 kg·m^{-2}·h^{-1} for a flow rate of 0.01 kg·s^{-1} to 16 kg·m^{-2}·h^{-1} for 0.005 kg·s^{-1} value of a flow, which means that the flow increased two times. From the obtained data and in order to guarantee the smooth running of the coupled system, 0.01 kg·s^{-1} was chosen as the optimum flow rate value.

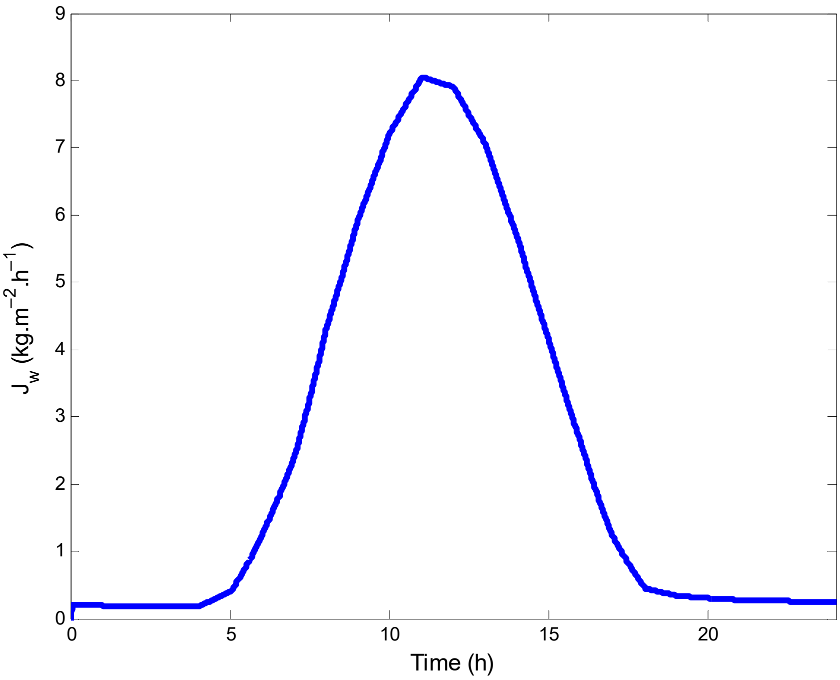

Figure 12. Variation of permeate flux over the local time.

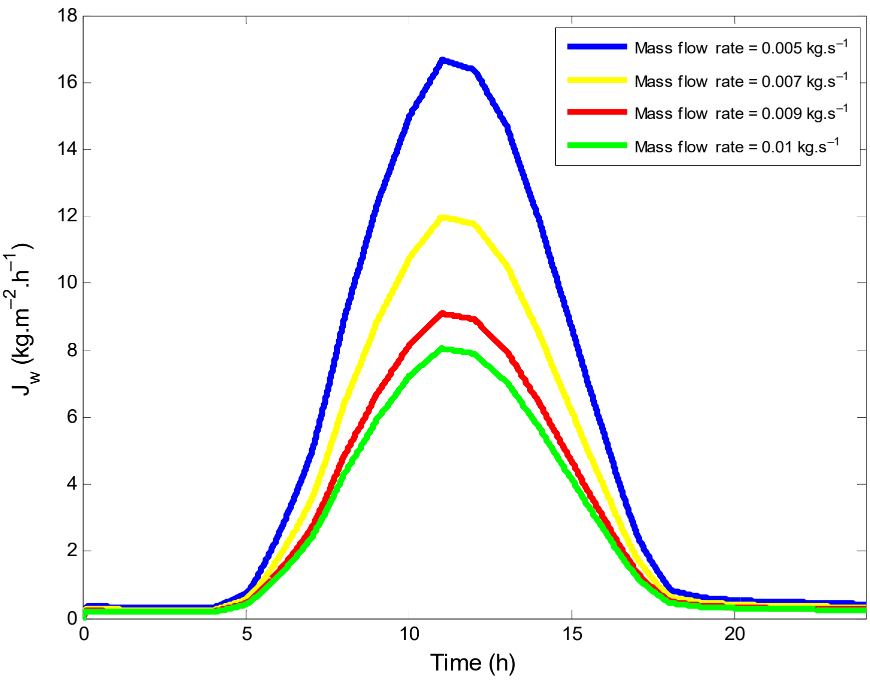

Figure 13. Variation of permeate flux of the different flow rates over the local time.

Air gap thickness is an important key. It plays a major role in the AGMD performance because the air gap is another additional resistance for the mass transfer to the AGMD process [13,14]. Figure 14 shows the effect of air gap thickness on permeate flow in intervals ranging from 1 to 3 mm. The influence of the air gap thickness was studied at a constant feed concentration of groundwater of 3.5 g·L^{-1}, while the flow rates of feed and coolant were kept constant at 2 L·min^{-1}. The increased air gap thickness in the module at the permeate side, caused by the higher mass transfer resistance, greatly reduces the permeate flux. Additionally, the performance of the AGMD process is directly influenced by the minimum air gap thickness.

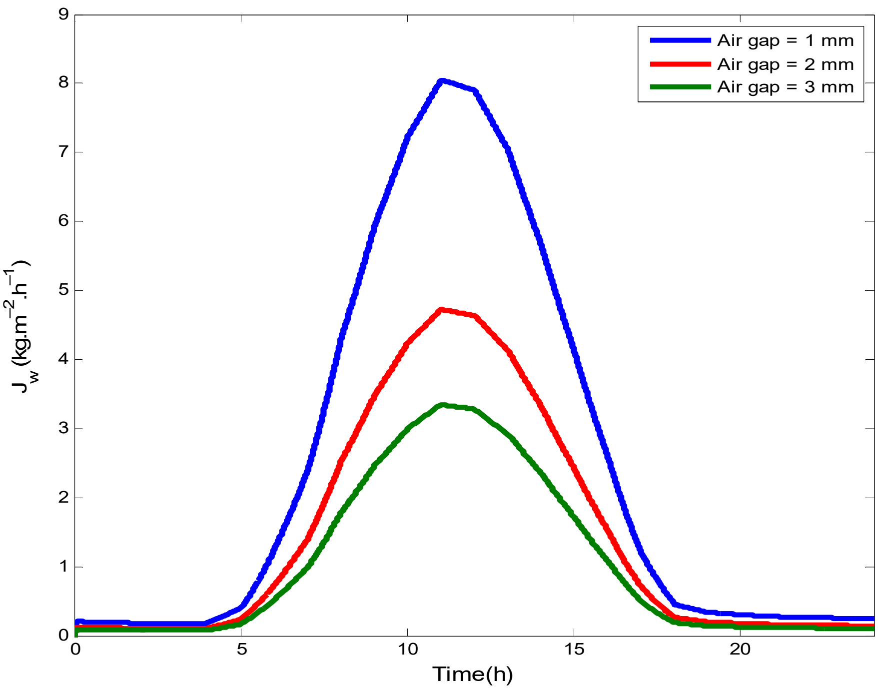

Figure 14. Variation of permeate flux with time at different air gap thicknesses.

4.6. System Performance

For each thermal desalination system, the evaluation of the principal parameters, such as GOR and PR, constitutes an important stage in the process of obtaining fresh water. Although, the greater the GOR or PR, the more effective thermal energy is used [56,57]. Figure 15 depicts the variation of GOR and PR as a function of local time. It can be observed from this figure that the GOR increases proportionally with the temperature difference across the AGMD membrane enhanced because of the increase in the amount of thermal energy needed for heating the water feed. However, as the feed temperature increases, the permeate flux increases exponentially, while the thermal energy consumption for heating the water solution feed increases. The maximum value of GOR = 4.6 is recorded at 12:00 h, mainly because of the maximum value of the hourly pure water productivity of the solar AGMD unit, which corresponds to the minimum irreversible loss of the whole desalination system.

In addition, the PR increases as the inlet temperature of the hot fluid increases. Similar behavior is observed for the GOR and reaches a maximum value of (PR = 2) at around 12:00 h. In addition, it was noticed that the influence of the calculated change in the latent heat of vaporization as a function of the hot fluid inlet temperature is negligible. However, the flow rate of the produced water increases more sharply than the energy consumption. The high PR indicated that a high flow rate of distillate is obtained for a given thermal energy input. Generally, high PR required some conditions, such as well-designed system components, high-energy efficiency, and good insulating material.

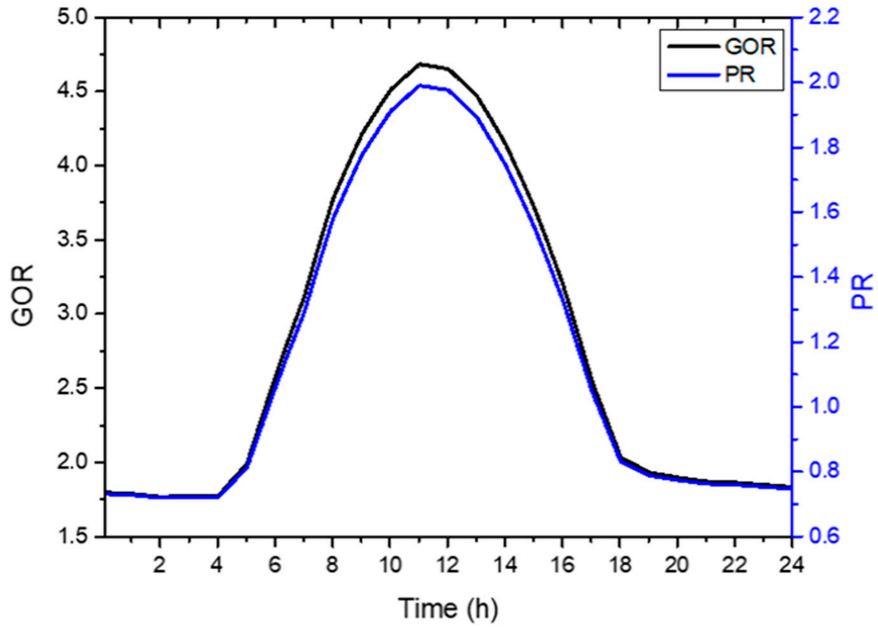

Figure 15. Variation of GOR and PR with time.

The GOR value in the literature ranges between 0.3 and 8.1, due to varying system design and operating conditions [58]. Table 2 summarizes the values gain output ratio obtained in the most common desalination technologies.

Table 2. Summary of gain output ratio for different MD configurations from the literature.

Type	GOR	Reference
AGMD	4.8	[59]
AGMD	4	[8]
MD	5.5	[50]
MD/MED	4.2	[58]
DCMD	0.3–0.9	[60]
AGMD	4.6	Current study

5. Conclusions

Solar energy use is an alternative, sustainable, and eco-green approach for saline water desalination. This study investigated the solar energy potential combined with an AGMD system for saline water desalination in the Sahara, in the Ghardaïa region (south of Algeria). A one-dimensional dynamic model of the heat and mass transfer processes in an AGMD process coupled to a flat plate collector was developed to predict flux and water production. The proposed model is validated against flux experimental data reported in the literature. Additionally, the study elucidated the effects of selected parameters on the efficiency of solar AGMD desalination systems. Therefore, from the obtained results the following conclusions can be drawn:

- The variation of the temperature of the heat transfer fluid at the outlet of the solar SFPC increases gradually to reach 50 °C, which is the most used value in the literature for the AGMD process and the collector's safety.
- An average distillate water production of 8 kg·m^{-2}·h^{-1} could be achieved at 68 °C for a feed temperature and a flow rate of 1 L·min^{-1}.
- Enhanced air gap thickness will be conducted to thermal and mass resistance, and thus a decrease in the mass flux and the thermal efficiency of the AGMD.
- The maximum GOR and PR values of 4.6 and 2, respectively, can be reached at 12:00 h corresponding to the minimum irreversible loss of the overall desalination system.

Finally, it should be noted that fouling can occur on the membrane surface, which reduce the permeate flux and affect the separation efficiency of AGMD. The air gap can also become fouled, further reducing the process performance. As a recommendation, further research should be conducted to investigate the impact of a membrane fouling mechanism on AGMD efficiency. Additionally, further optimization of the solar AGMD desalination system is possible taking into account the economic and environmental aspects by using exergoeconomic and exergoenvironmental approaches.

Author Contributions: Conceptualization, N.M., A.-E.B. and H.T.; methodology, Z.T. and M.K.; software, H.T. and Z.T.; validation, L.M., A.A. and M.Z.; formal analysis, M.K. and M.Z.; investigation, N.M. and A.-E.B.; resources, A.A.; data curation, H.T.; writing—original draft preparation, N.M., L.M. and A.-E.B.; writing—review and editing, L.M. and A.-E.B.; visualization, L.M., A.A. and A.-E.B.; supervision, L.M.; project administration, H.T. and J.Z. All authors have read and agreed to the published version of the manuscript.

Funding: This research received no external funding.

Institutional Review Board Statement: Not applicable.

Informed Consent Statement: Not applicable.

Data Availability Statement: Not applicable.

Acknowledgments: This work was supported in entirely by the Biomaterials and Transport Phenomena Laboratory agreement N° 303 12 March 2003, at the University of Medea. The authors acknowledge and gratefully thank the financial support provided by DG-RSDT of Algeria.

Conflicts of Interest: The authors declare no conflict of interest.

Nomenclature

A	surface area [m^2]
B_w	mass transfer coefficient [kg·m^{-2}·h^{-1}·Pa^{-1}]
C_p	thermal capacity [J·kg^{-1}·K^{-1}]
D_{va}	thermal diffusivity of water vapour in air [m^2·s^{-1}]
d_h	hydraulic diameter [m]
F	correction factor [−]
F_R	heat removal factor [−]
GOR	gained output ratio [−]
hc_c	heat transfer coefficient [W·m^{-2}·K^{-1}]
h_{ch}	convective heat transfer coefficient [W·m^{-2}·K^{-1}]
h_v	enthalpy [kJ·kg^{-1}]
J_w	permeate flux [kg·m^{-2}·s^{-1}]
k	thermal conductivity [W·m^{-1}·K^{-1}]
L	module length [m]
LMDT	logarithmic mean temperature difference [K]
M_w	Molar mass of water [kg·mol^{-1}]
$\dot{m}$	mass flow rate [kg·s^{-1}]
MED	multiple-effect distillation
MD	membrane distillation
MSF	multi-stage flash distillation
P	pressure [Pa]
PR	Performance Ratio [−]
Q_u	useful energy delivered by the solar collector [kW]
φ	thermal flux [W·m^{-2}]
R	thermal resistance [m^2·K·W^{-1}]
RO	reverse osmosis
s	salinity [g·kg^{-1}]
T	temperature [°C]
t	time [s]
U	heat transfer coefficient [W·m^{-2}·K^{-1}]

VMD	vacuum membrane distillation
Greek letters	
α	activity coefficient [−]
β	water fraction [−]
δ	thickness [m]
ε	porosity [−]
μ	dynamic viscosity [kg·m^{-1}·s^{-1}]
ρ	density [kg·m^{-3}]
φ	thermal flux [W·m^{-2}]
τ	tortuosity [−]
Subscripts	
0	reference state
a	air
ag	air gap
c	cold
f	feed
h	hot
h_m	hot fluid—membrane interface
in	inlet
m	membrane
mg	membrane—air gap interface
out	outlet
p	plate
m_g	membrane—air gap interface
pc	cold fluid—plate interface
r	receiver
so	source
sw	seawater
th	thermal
v	vapour

References

1. Kumar, A.; Saini, R.P.; Saini, J.S. A Review of Thermohydraulic Performance of Artificially Roughened Solar Air Heaters. *Renew. Sustain. Energy Rev.* **2014**, *37*, 100–122. [CrossRef]
2. Bayrak, F.; Oztop, H.F.; Hepbasli, A. Energy and Exergy Analyses of Porous Baffles Inserted Solar Air Heaters for Building Applications. *Energy Build.* **2013**, *57*, 338–345. [CrossRef]
3. Yang, Y.; Wang, Q.; Xiu, D.; Zhao, Z.; Sun, Q. A Building Integrated Solar Collector: All-Ceramic Solar Collector. *Energy Build.* **2013**, *62*, 15–17. [CrossRef]
4. Zhai, X.Q.; Wang, R.Z.; Dai, Y.J.; Wu, J.Y.; Xu, Y.X.; Ma, Q. Solar Integrated Energy System for a Green Building. *Energy Build.* **2007**, *39*, 985–993. [CrossRef]
5. Djellouli-Tabet, Y. Common Scarcity, Diverse Responses in the Maghreb Region. In *Water and Sustainability in Arid Regions: Bridging the Gap Between Physical and Social Sciences*; Springer: Heidelberg, Germany, 2010; pp. 87–102.
6. Rabehi, A.; Guermoui, M.; Djafer, D.; Zaiani, M. Radial Basis Function Neural Networks Model to Estimate Global Solar Radiation in Semi-Arid Area. *Leonardo Electron. J. Pract. Technol.* **2015**, *27*, 177–184.
7. Al-Obaidani, S.; Curcio, E.; Macedonio, F.; Di Profio, G.; Al-Hinai, H.; Drioli, E. Potential of Membrane Distillation in Seawater Desalination: Thermal Efficiency, Sensitivity Study and Cost Estimation. *J. Membr. Sci.* **2008**, *323*, 85–98. [CrossRef]
8. Diaby, A.T.; Byrne, P.; Loulergue, P.; Balannec, B.; Szymczyk, A.; Maré, T.; Sow, O. Design Study of the Coupling of an Air Gap Membrane Distillation Unit to an Air Conditioner. *Desalination* **2017**, *420*, 308–317. [CrossRef]
9. Banat, F.; Jwaied, N.; Rommel, M.; Koschikowski, J.; Wieghaus, M. Desalination by a "Compact SMADES" Autonomous Solarpowered Membrane Distillation Unit. *Desalination* **2007**, *217*, 29–37. [CrossRef]
10. Banat, F.; Jwaied, N.; Rommel, M.; Koschikowski, J.; Wieghaus, M. Performance Evaluation of the "Large SMADES" Autonomous Desalination Solar-Driven Membrane Distillation Plant in Aqaba, Jordan. *Desalination* **2007**, *217*, 17–28. [CrossRef]
11. Chafidz, A.; Al-Zahrani, S.; Al-Otaibi, M.N.; Hoong, C.F.; Lai, T.F.; Prabu, M. Portable and Integrated Solar-Driven Desalination System Using Membrane Distillation for Arid Remote Areas in Saudi Arabia. *Desalination* **2014**, *345*, 36–49. [CrossRef]
12. Wang, Y.; Xu, Z.; Lior, N.; Zeng, H. An Experimental Study of Solar Thermal Vacuum Membrane Distillation Desalination. *Desalin. Water Treat.* **2015**, *53*, 887–897. [CrossRef]
13. Guillén-Burrieza, E.; Zaragoza, G.; Miralles-Cuevas, S.; Blanco, J. Experimental Evaluation of Two Pilot-Scale Membrane Distillation Modules Used for Solar Desalination. *J. Membr. Sci.* **2012**, *409*, 264–275. [CrossRef]
14. Suárez, F.; Tyler, S.W.; Childress, A.E. A Theoretical Study of a Direct Contact Membrane Distillation System Coupled to a Salt-Gradient Solar Pond for Terminal Lakes Reclamation. *Water Res.* **2010**, *44*, 4601–4615. [CrossRef] [PubMed]
15. Wang, X.; Zhang, L.; Yang, H.; Chen, H. Feasibility Research of Potable Water Production via Solar-Heated Hollow Fiber Membrane Distillation System. *Desalination* **2009**, *247*, 403–411. [CrossRef]
16. Banat, F.; Jumah, R.; Garaibeh, M. Exploitation of Solar Energy Collected by Solar Stills for Desalination by Membrane Distillation. *Renew. Energy* **2002**, *25*, 293–305. [CrossRef]
17. Vickers, N.J. Animal Communication: When i'm Calling You, Will You Answer Too. *Curr. Biol.* **2017**, *27*, R713–R715. [CrossRef]
18. Qtaishat, M.R.; Banat, F. Desalination by Solar Powered Membrane Distillation Systems. *Desalination* **2013**, *308*, 186–197. [CrossRef]
19. Banat, F.; Jwaied, N. Economic Evaluation of Desalination by Small-Scale Autonomous Solar-Powered Membrane Distillation Units. *Desalination* **2008**, *220*, 566–573. [CrossRef]
20. Guillén-Burrieza, E.; Blanco, J.; Zaragoza, G.; Alarcón, D.-C.; Palenzuela, P.; Ibarra, M.; Gernjak, W. Experimental Analysis of an Air Gap Membrane Distillation Solar Desalination Pilot System. *J. Membr. Sci.* **2011**, *379*, 386–396. [CrossRef]
21. Kubota, S.; Ohta, K.; Hayano, I.; Hirai, M.; Kikuchi, K.; Murayama, Y. Experiments on Seawater Desalination by Membrane Distillation. *Desalination* **1988**, *69*, 19–26. [CrossRef]
22. Summers, E.K.; Lienhard, V.J.H. A Novel Solar-Driven Air Gap Membrane Distillation System. *Desalin. Water Treat.* **2013**, *51*, 1344–1351. [CrossRef]
23. Moudjeber, D.-E.; Ruiz-Aguirre, A.; Ugarte-Judge, D.; Mahmoudi, H.; Zaragoza, G. Solar Desalination by Air-Gap Membrane Distillation: A Case Study from Algeria. *Desalin. Water Treat.* **2016**, *57*, 22718–22725. [CrossRef]
24. Kumar, N.U.; Martin, A. Experimental Modeling of an Air-Gap Membrane Distillation Module and Simulation of a Solar Thermal Integrated System for Water Purification. *Water Treat.* **2017**, *84*, 123–134.
25. Shirsath, G.B.; Muralidhar, K.; Pala, R.G.S. Variable Air Gap Membrane Distillation for Hybrid Solar Desalination. *J. Environ. Chem. Eng.* **2020**, *8*, 103751. [CrossRef]
26. SANDİD, A.; Nehari, D.; Elmeriah, A.; Remlaoui, A. Dynamic Simulation of an Air-Gap Membrane Distillation (AGMD) Process Using Photovoltaic Panels System and Flat Plate Collectors. *J. Therm. Eng.* **2021**, *7*, 117–133. [CrossRef]
27. Sandida, A.M.; Neharia, T.; Neharia, D. Simulation Study of an Air-Gap Membrane Distillation System for Seawater Desalination Using Solar Energy. *Desalin. Water Treat.* **2021**, *229*, 40–51. [CrossRef]
28. Sandid, A.M.; Bassyouni, M.; Nehari, D.; Elhenawy, Y. Experimental and Simulation Study of Multichannel Air Gap Membrane Distillation Process with Two Types of Solar Collectors. *Energy Convers. Manag.* **2021**, *243*, 114431. [CrossRef]
29. Thai Huynh, N.V.T.; Nguyen, T.; Manh Nguyen, Q. Optimum Design for the Magnification Mechanisms Employing Fuzzy Logic–ANFIS. *Comput. Mater. Contin.* **2022**, *73*, 5961–5983. [CrossRef]

30. Wang, C.-N.; Yang, F.-C.; Nguyen, V.T.T.; Nguyen, Q.M.; Huynh, N.T.; Huynh, T.T. Optimal Design for Compliant Mechanism Flexure Hinges: Bridge-Type. *Micromachines* **2021**, *12*, 1304. [CrossRef]
31. Wang, C.-N.; Yang, F.-C.; Nguyen, V.T.T.; Vo, N.T.M. CFD Analysis and Optimum Design for a Centrifugal Pump Using an Effectively Artificial Intelligent Algorithm. *Micromachines* **2022**, *13*, 1208. [CrossRef]
32. Khalifa, A.E.; Lawal, D.U. Performance and Optimization of Air Gap Membrane Distillation System for Water Desalination. *Arab. J. Sci. Eng.* **2015**, *40*, 3627–3639. [CrossRef]
33. Dudchenko, A.V.; Bartholomew, T.V.; Mauter, M.S. Cost Optimization of Multi-Stage Gap Membrane Distillation. *J. Membr. Sci.* **2021**, *627*, 119228. [CrossRef]
34. Chen, Y.-H.; Li, Y.-W.; Chang, H. Optimal Design and Control of Solar Driven Air Gap Membrane Distillation Desalination Systems. *Appl. Energy* **2012**, *100*, 193–204. [CrossRef]
35. Khayet, M.; Cojocaru, C. Air Gap Membrane Distillation: Desalination, Modeling and Optimization. *Desalination* **2012**, *287*, 138–145. [CrossRef]
36. Khayet, M.; Cojocaru, C. Artificial Neural Network Modeling and Optimization of Desalination by Air Gap Membrane Distillation. *Sep. Purif. Technol.* **2012**, *86*, 171–182. [CrossRef]
37. He, Q.; Li, P.; Geng, H.; Zhang, C.; Wang, J.; Chang, H. Modeling and Optimization of Air Gap Membrane Distillation System for Desalination. *Desalination* **2014**, *354*, 68–75. [CrossRef]
38. Diaby, A.T.; Byrne, P.; Loulergue, P.; Sow, O.; Maré, T. Experimental Study of a Heat Pump for Simultaneous Cooling and Desalination by Membrane Distillation. *Membranes* **2021**, *11*, 725. [CrossRef]
39. Khalifa, A.; Ahmad, H.; Antar, M.; Laoui, T.; Khayet, M. Experimental and Theoretical Investigations on Water Desalination Using Direct Contact Membrane Distillation. *Desalination* **2017**, *404*, 22–34. [CrossRef]
40. Boubakri, A.; Hafiane, A.; Al Tahar Bouguecha, S. Nitrate Removal from Aqueous Solution by Direct Contact Membrane Distillation Using Two Different Commercial Membranes. *Desalin. Water Treat.* **2015**, *56*, 2723–2730. [CrossRef]
41. Irshad, M.; Yadav, A.; Singh, R.; Kumar, A. Mathematical Modelling and Performance Analysis of Single Pass Flat Plate Solar Collector. *IOP Conf. Ser. Mater. Sci. Eng.* **2018**, *404*, 012051. [CrossRef]
42. Ismail, T. Study, Realization and Simulation of a Solar Collector. Ph.D. Thesis, Universite Des FreresMentouri, Constantine, Algeria, 2016.
43. Terfai, A.; Chiba, Y.; Zirari, M.; Bouaziz, M.N. Numerical Simulation of a Flat-Plate Solar Collector Operating Under Open Cycle Mode of Heat Extraction. In *Proceedings of the Advances in Green Energies and Materials Technology: Selected Articles from the Algerian Symposium on Renewable Energy and Materials (ASREM-2020)*; Springer: Heidelberg, Germany, 2021; pp. 153–158.
44. Zelzouli, K.; Guizani, A.; Sebai, R.; Kerkeni, C. Solar Thermal Systems Performances versus Flat Plate Solar Collectors Connected in Series. *Engineering* **2012**, *4*, 881–893. [CrossRef]
45. Koschikowski, J.; Wieghaus, M.; Rommel, M. Solar Thermal-Driven Desalination Plants Based on Membrane Distillation. *Desalination* **2003**, *156*, 295–304. [CrossRef]
46. Fane, A.G.; Schofield, R.W.; Fell, C.J.D. The Efficient Use of Energy in Membrane Distillation. *Desalination* **1987**, *64*, 231–243. [CrossRef]
47. Alsaadi, A.S.; Ghaffour, N.; Li, J.-D.; Gray, S.; Francis, L.; Maab, H.; Amy, G.L. Modeling of Air-Gap Membrane Distillation Process: A Theoretical and Experimental Study. *J. Membr. Sci.* **2013**, *445*, 53–65. [CrossRef]
48. Banat, F.A. Membrane Distillation for Desalination and Removal of Volatile Organic Compounds from Water. Ph.D. Thesis, McGill University, Montreal, QC, Canada, 1994.
49. Garci-Payo, M.C. MA Lzquierdo-Gill and C. Fernandez-Pineda. *J. Membr. Sci* **2000**, *169*, 61.
50. Safavi, M.; Mohammadi, T. High-Salinity Water Desalination Using VMD. *Chem. Eng. J.* **2009**, *149*, 191–195. [CrossRef]
51. Martinez-Diez, L.; Florido-Diaz, F.J.; Vazquez-Gonzalez, M.I. Study of Evaporation Efficiency in Membrane Distillation. *Desalination* **1999**, *126*, 193–198. [CrossRef]
52. Schofield, R.W.; Fane, A.G.; Fell, C.J.D.; Macoun, R. Factors Affecting Flux in Membrane Distillation. *Desalination* **1990**, *77*, 279–294. [CrossRef]
53. Yun, Y.; Ma, R.; Zhang, W.; Fane, A.G.; Li, J. Direct Contact Membrane Distillation Mechanism for High Concentration NaCl Solutions. *Desalination* **2006**, *188*, 251–262. [CrossRef]
54. Gairaa, K.; Bakelli, Y. Solar Energy Potential Assessment in the Algerian South Area: Case of Ghardaïa Region. *J. Renew. Energy* **2013**, *2013*, 496348. [CrossRef]
55. Al-Zoubi, H.; Al-Amri, F.; Khalifa, A.E.; Al-Zoubi, A.; Muhammad, A.; Ebtehal, Y.; Mallick, T.K. A Comprehensive Review of Air Gap Membrane Distillation Process. *Desalin. Water Treat.* **2018**, *110*, 27–64. [CrossRef]
56. Rahimi-Ahar, Z.; Hatamipour, M.S.; Ahar, L.R. Air Humidification-Dehumidification Process for Desalination: A Review. *Prog. Energy Combust. Sci.* **2020**, *80*, 100850. [CrossRef]
57. Zheng, H. *Solar Energy Desalination Technology*; Elsevier: Amsterdam, The Netherlands, 2017; ISBN 0-12-809422-2.
58. De Andrés, M.C.; Doria, J.; Khayet, M.; Peña, L.; Mengual, J.I. Coupling of a Membrane Distillation Module to a Multieffect Distiller for Pure Water Production. *Desalination* **1998**, *115*, 71–81. [CrossRef]

59. Camacho, L.M.; Dumée, L.; Zhang, J.; Li, J.; Duke, M.; Gomez, J.; Gray, S. Advances in Membrane Distillation for Water Desalination and Purification Applications. *Water* **2013**, *5*, 94–196. [CrossRef]
60. Alquraish, M.M.; Mejbri, S.; Abuhasel, K.A.; Zhani, K. Experimental Investigation of a Pilot Solar-Assisted Permeate Gap Membrane Distillation. *Membranes* **2021**, *11*, 336. [CrossRef]